The Astrophysical Journal, 821:79 (9pp), 2016 April 20 doi:10.3847/0004-637X/821/2/79

X-RAY OBSERVATIONS OF BOW SHOCKS AROUND RUNAWAY O STARS. THE CASE OF ζ OPH AND BD+43°3654

J. A. Toalá[1,2], L. M. Oskinova[3], A. González-Galán[3], M. A. Guerrero[1], R. Ignace[4], and M. Pohl[2,3,5]
[1] Instituto de Astrofísica de Andalucía, IAA-CSIC, Glorieta de la Astronomía s/n, E-18008 Granada, Spain; toala@iaa.es
[2] Institute of Astronomy and Astrophysics, Academia Sinica (ASIAA), Taipei 10617,Taiwan
[3] Institute for Physics and Astronomy, University of Potsdam, D-14476 Potsdam, Germany
[4] Department of Physics and Astronomy, East Tennessee State University, Johnson City, TN 37614, USA
[5] DESY, Platanenallee 6, D-15738 Zeuthen, Germany
Received 2016 January 3; accepted 2016 February 24; published 2016 April 13

ABSTRACT

Non-thermal radiation has been predicted within bow shocks around runaway stars by recent theoretical works. We present X-ray observations toward the runaway stars ζ Oph by *Chandra* and *Suzaku* and of BD+43°3654 by *XMM-Newton* to search for the presence of non-thermal X-ray emission. We found no evidence of non-thermal emission spatially coincident with the bow shocks; nonetheless, diffuse emission was detected in the vicinity of ζ Oph. After a careful analysis of its spectral characteristics, we conclude that this emission has a thermal nature with a plasma temperature of $T \approx 2 \times 10^6$ K. The cometary shape of this emission seems to be in line with recent predictions of radiation-hydrodynamic models of runaway stars. The case of BD+43°3654 is puzzling, as non-thermal emission has been reported in a previous work for this source.

Key words: stars: individual (ζ Oph, BD+43°3654) – stars: winds, outflows

1. INTRODUCTION

Runaway stars are thought to be ejected from their formation nursery with high velocities ($v_* \gtrsim 30\,\mathrm{km\,s^{-1}}$; Gies & Bolton 1986; Tetzlaff et al. 2011). The origin of these high velocities is still a matter of debate. Some possibilities include the effects of close interactions between binary systems in a cluster (e.g., Hoogerwerf et al. 2000), strong gravitational interactions between single and binary systems (e.g., Fujii & Portegies Zwart 2011), or kicks arising from a supernova explosion of a binary companion (e.g., Blaauw 1961).

Runaway massive ($M > 10\,M_\odot$) stars moving supersonically through the interstellar medium (ISM) produce large-scale bow shocks. The gas and dust compressed in bow shocks is heated and ionized by the intense stellar radiation, making these large-scale ISM structures observable in infrared (IR) and in optical (e.g., Hα) emission (e.g., van Buren & McCray 1988). Indeed, many stellar bow shocks have been detected in optical and IR wavelengths (e.g., van Buren et al. 1995; Kaper et al. 1997; Noriega-Crespo et al. 1997; Kobulnicky et al. 2010; Peri et al. 2012). Nevertheless, there are certain physical conditions in which a stellar bow shock may not form. For example, if the star is moving with sub-sonic velocities in a too tenuous, hot ambient medium or if it has a weak wind or a high space velocity (e.g., Comeron & Kaper 1998; Huthoff & Kaper 2002).

Bow shocks around massive stars are also detected at radio wavelengths. Benaglia et al. (2010) reported, for the first time, radio emission from the bow shock around a massive runaway star (BD+43°3654). Their Very Large Array (VLA) observations provided stark evidence that non-thermal radio emission is spatially coincident with the bow shock observed in infrared emission. Benaglia et al. (2010) argued that this non-thermal emission should arise from the cooling of energetic electrons by syncrotron emission. The electrons that produce this non-thermal radio emission could upscatter photons from the stellar and dust photon fields via the inverse Compton process, leading to high-energy emission. In particular, inverse Compton scattering into the X-ray band requires very low-energy electrons with Lorentz factors of the order of 100.

Since this discovery, a number of theoretical works have been presented to address the production of non-thermal emission at the position of the bow shock around runaway stars (see del Valle et al. 2015, and references therein). del Valle & Romero (2012) presented analytical calculations with applications to the closest runaway massive O-type star, ζ Oph, and concluded that non-thermal X-ray and γ-ray emission from its bow shock should be detectable. This work was farther extended by del Valle & Romero (2014), who presented the model spectral energy distribution over the broad range of energy.

The predictions of del Valle & Romero's model were observationally tested by Schulz et al. (2014). Using the analysis of data accumulated during 57 months by the *Fermi* γ-ray Space Telescope, the first systematic search of γ-ray emission from 27 bow shocks around runaway stars was performed. No positive detections were obtained. It was demonstrated that for the case of ζ Oph, the upper limit on its γ-ray emission was five times below that predicted by del Valle & Romero (2012). At the X-ray wavelengths, Terada et al. (2012) presented *Suzaku* observations of BD+43°3654 and did not detect non-thermal X-ray emission associated to its bow shock. Only one marginal detection of non-thermal X-ray emission from a bow shock around a runaway star has been reported to date. This detection was claimed by López-Santiago et al. (2012) for AE Aurigae (HIP 24575) using *XMM-Newton* observations. Unfortunately, the data did not discriminate between non-thermal and thermal emission.

Besides non-thermal radiation, X-rays from bow shocks originating in thermal plasma can be expected. A number of numerical simulations have shown that the stellar wind-ISM interaction resulting from both slow- and fast-moving stars produces instabilities that mix material between the adiabatically shocked wind and the photoionized gas at the wake of the bow shock (e.g., Brighenti & D'Ercole 1995a, 1995b; Arthur & Hoare 2006; Mackey et al. 2015; Meyer et al. 2015); this creates a mixing region capable of producing plasma

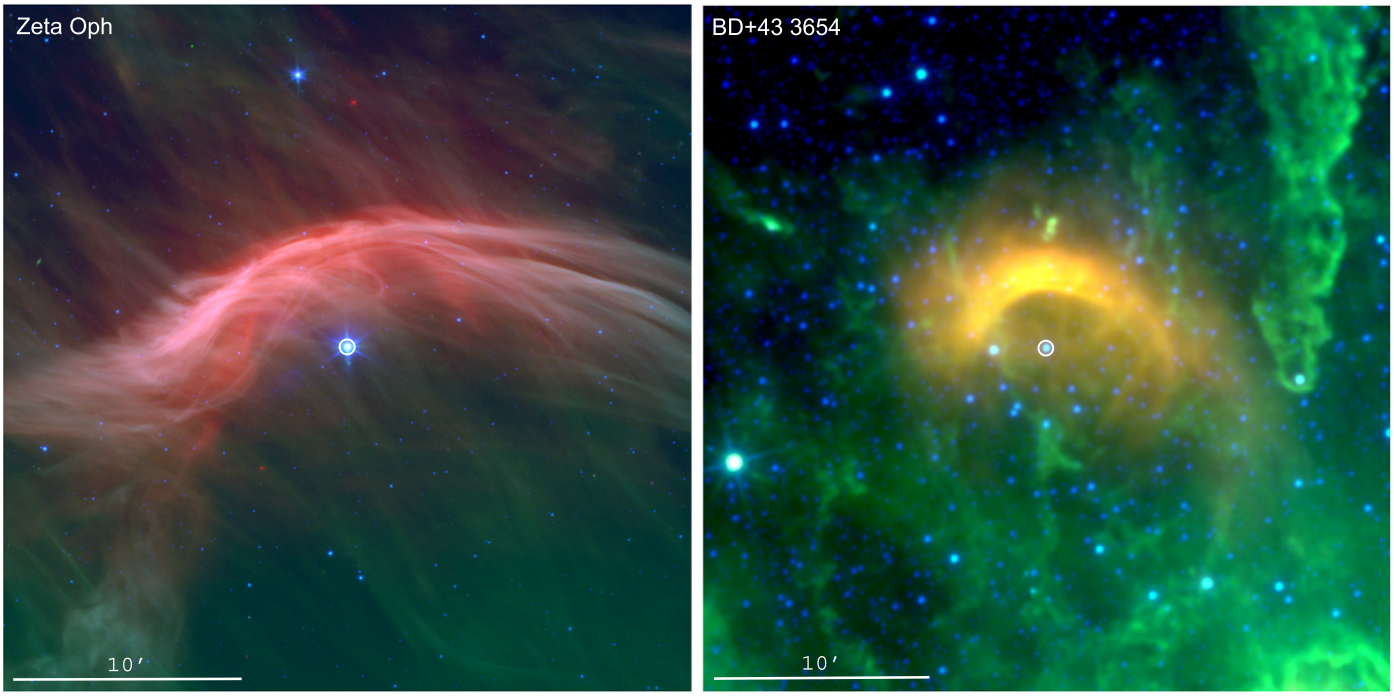

Figure 1. Composite color mid-IR images of ζ Oph (left panel) and BD+43°3654 (right panel). For ζ Oph, the red, green, and blue correspond to *Spitzer* MIPS 24 μm, IRAC 8 μm, and IRAC 4.5 μm, respectively. In the case of BD+43°3654, the red, green, and blue correspond to *WISE* 22, 12, and 4.6 μm, respectively. The circular aperture in both panels show the position of the central stars. North is up and East is left.

temperatures of $\sim 10^6$ K. In particular, Mackey et al. (2015) presented radiation-hydrodynamic simulations on the formation of bow shocks around massive O-type stars and showed that these instabilities are capable of producing diffuse X-ray emission at the wake.[6]

In this paper we present *Chandra*, *Suzaku*, and *XMM-Newton* observations toward the runaway O stars ζ Oph and BD+43°3654 to explore the existence of extended X-ray emission associated to their bow shocks and its nature. Both of these runaway stars display extended bow shocks seen in mid-infrared images (see Figure 1) and are relatively close and suffer only modest extinction, allowing to probe soft X-ray emission. This makes them the best candidates to test the predictions from theory.

The wind parameters of ζ Oph (O9.2IV) were derived by Marcolino et al. (2009) from modeling its optical and UV spectra, $\dot{M} \approx 1.6 \times 10^{-9}\, M_\odot$ yr^{-1}, and its terminal wind velocity, $v_\infty \approx 1500$ km s^{-1}, while Gvaramadze et al. (2012) find an order of magnitude higher mass-loss rate, $\dot{M} \approx 2 \times 10^{-8}\, M_\odot$ yr^{-1}, from the analysis of its bow shock. This discrepancy could be explained if the bulk of ζ Oph wind was in a hot phase (Huenemoerder et al. 2012). In this case, the wind kinetic power is $E_{\rm wind} \approx 1.4 \times 10^{34}$ erg s^{-1}.

From the analysis of the IR image of the bow shock around BD+43°3654 (O4If), Kobulnicky et al. (2010) found a very large mass-loss rate for this star, $\dot{M} \sim 2 \times 10^{-4}\, M_\odot$ yr^{-1}. However, they pointed out that this value is uncertain because of the poorly known ISM density around this object. The mass-loss rate of an O-type star with the same spectral type, ζ Pup (O4If(n)) is $\dot{M} \approx 2.5 \times 10^{-6}\, M_\odot$ yr^{-1}, and wind velocity, $v_\infty \approx 2250$ km s^{-1} (Oskinova et al. 2007; Šurlan et al. 2013). Adopting these parameters results in a wind power of $E_{\rm wind} \approx 4 \times 10^{36}$ erg s^{-1}.

[6] Note, however, that the simulations presented by Mackey et al. (2015) are tailored to runaway stars with velocities $v_\star = 4$–16 km s^{-1}.

The structure of the paper is as follows. In Section 2 we describe the X-ray observations. Section 3 describes the results and spectral analysis. We discuss our findings and present our conclusions in Sections 4 and 5, respectively.

2. OBSERVATIONS

2.1. ζ Oph

The *Chandra* observations of ζ Oph were performed on 2013 July 3 (Observation ID: 14540; PI: L.M. Oskinova) using the Advanced CCD Imaging Spectrometer (ACIS-I) for a total exposure time of 72.1 ks. The *Chandra* Interactive Analysis of Observations (CIAO) software package version 4.6 (Fruscione et al. 2006) was used to analyze the data using CALB version 4.6.3. The resulting exposure time after excising dead time periods is 71.8 ks. The left panel of Figure 2 presents the field of view (FOV) of the ACIS-I observations in the 0.25–8.0 keV energy range. Several point-like sources can be identified as well as a diffuse source toward the northeast of the FOV of the ACIS-I detectors with its maximum located at (R.A., decl.) = ($16^{\rm h}\ 37^{\rm m}\ 44\overset{\rm s}{.}2$, $-10°\ 27'\ 17\overset{''}{.}1$). This source is spatially coincident with 1AXG J163740–1027 as reported in the *ASCA* Medium Sensitivity Survey by Ueda et al. (2001) within the error reported by those authors.

Exposure-corrected, background-subtracted images of the soft (0.25–1.0 keV), medium (1.0–2.0 keV), and hard (2.0–8.0 keV) X-ray images are presented in Figure 3. Point-like sources have been removed and the gaps have been filled with the CIAO task *dmfilth*. The final images were smoothed with the CIAO task *aconvolve*, with a Gaussian kernel of 4″ in the brightest regions. A composite color picture of the three images is presented in the bottom right panel of Figure 3. White contours show the distribution of the MIPS 24 μm emission around ζ Oph.

We also used *Suzaku* observations of ζ Oph to complement our study. These observations were performed on 2008 March

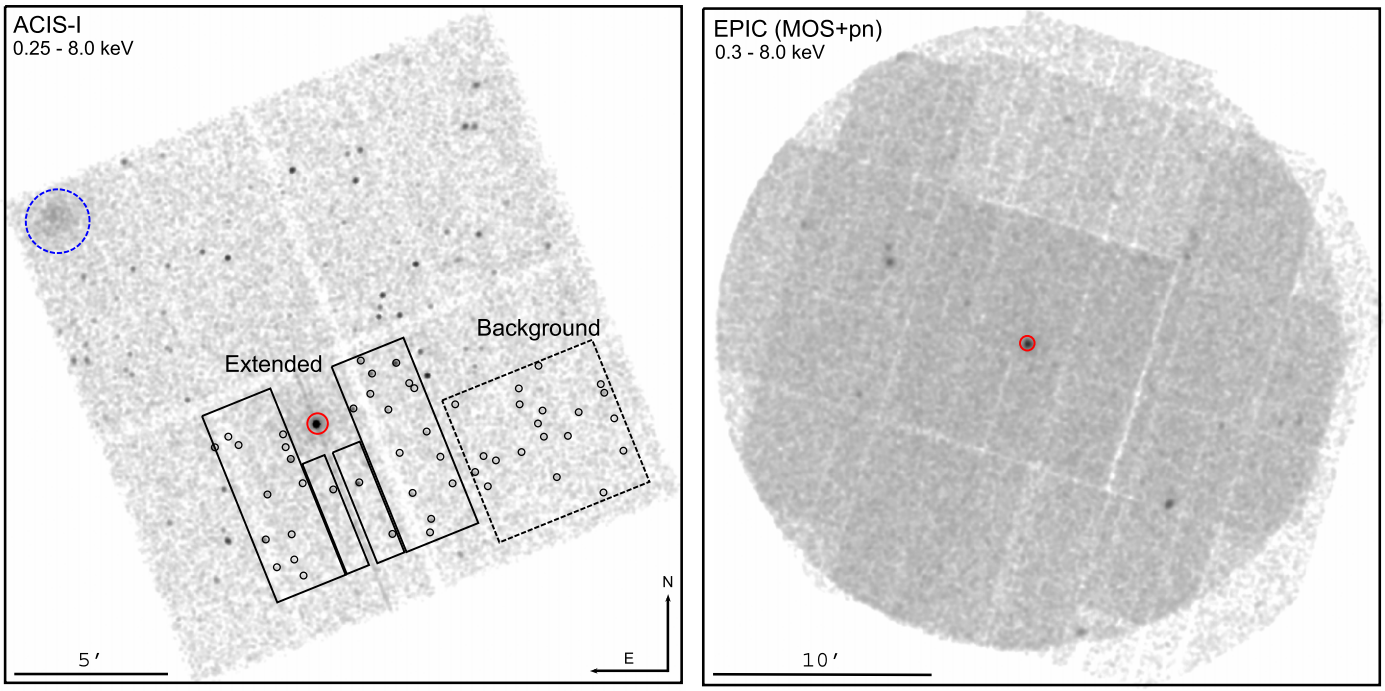

Figure 2. FOV of the X-ray observations toward ζ Oph and BD+43°3654. Left: *Chandra* ACIS-I smoothed exposure-corrected image of ζ Oph in the 0.25–8.0 keV energy range. Right: *XMM-Newton* EPIC (MOS+pn) smoothed exposure-corrected image of BD+43°3654 in the 0.3–8.0 keV energy range. The (red) solid line circle on each panel indicates the spectrum extraction region of the target stars. Other point-like sources in the FOV have been identified. The blue dashed-line circular aperture in the left panel shows the position of the diffuse extragalactic source 1AXG J163740–1027 (see the text).

15 (Observation ID: 402038010; PI: W.L. Waldron) using the X-ray Imaging Spectrometers XIS 0, XIS 1, and XIS 3. The net exposure times for each camera are 95.7 ks. Due to their lower angular resultion, no spatial distribution of the X-ray-emitting gas can be performed from these cameras. We only used the *Suzaku* observations to perform the spectral study of ζ Oph (see Section 3.1). To illustrate this, we show the smoothed exposure-corrected image of the Suzaku XIS 1 in the Appendix.

2.2. BD+43°3654

The *XMM-Newton* observations toward BD+43°3654 were performed in 2010 May 8 (Observation ID: 0653690101; PI: V. Zabalza). The EPIC cameras were operated in the full-frame mode with the thin optical filter for a total exposure time of 38.5, 45.7, 45.7 ks for the EPIC-pn, MOS1, and MOS2 cameras, respectively. The observations were processed using the *XMM-Newton* Science Analysis Software (SAS version 13.5.0) with the associated calibration files (CCF) available on 2014 October 28. The right panel of Figure 2 shows the FOV of the EPIC observations in the 0.3–8.0 keV energy range. Unfortunately, these observations were severely affected by high background levels and the final net exposure times are 7.0, 23.5, and 26.6 ks for the EPIC-pn, MOS1, and MOS2 cameras, respectively. We note that Terada et al. (2012) have used these *XMM-Newton* observations to search for point-like sources in the FOV of their *Suzaku* observations of BD+43°3654. However, they did not perform further analysis of the *XMM-Newton* data.

Exposure-corrected, background-subtracted images at different bands (namely soft 0.3–1.0 keV, medium 1.0–2.0 keV, and hard 2.0–8.0 keV bands) were generated using the ESAS-XMM tasks. The final images have been adaptively smoothed using the ESAS-XMM task *adapt* requesting 50 counts for the three bands (see Figure 4). A composite color picture of the three images is presented in the bottom right panel of Figure 4. White contours show the distribution of the *WISE* 22 μm emission around BD+43°3654.

3. RESULTS

As expected, both central stars are detected in X-rays. Figures 3 and 4 show the spatial distribution of the X-ray emission around our targets. As can be seen in Figure 3, the *Chandra* images show that diffuse X-ray emission is present close to ζ Oph, spatially coinciding with the likely location of the bow shock wake. On the other hand, we find no extended X-ray emission associated with the bow shock apex.

Figure 4 corroborates the findings presented by Terada et al. (2012), who did not find any hint of diffuse X-ray emission associated with the bow shock around BD+43°3654 in their *Suzaku* observations.

3.1. X-Rays from ζ Oph

We carefully examined the *Chandra* images of ζ Oph for the different energies and in full band to search for traces of diffuse emission associated with the bow shock. However, no such emission was detected. Hence, if any X-ray emission directly associated to the bow shock should exist, it shall be below the background level (see Section 4).

To study the physical properties of the X-ray emission from ζ Oph and the apparent extended emission around it, we have extracted two spectra from the *Chandra* ACIS-I observations. A circular aperture with a radius of 20″ has been used to extract a spectrum from ζ Oph, while the corresponding spectrum from the diffuse emission has been extracted from the polygonal apertures shown in the left panel of Figure 2. The background region for both spectra has been selected from a region with no

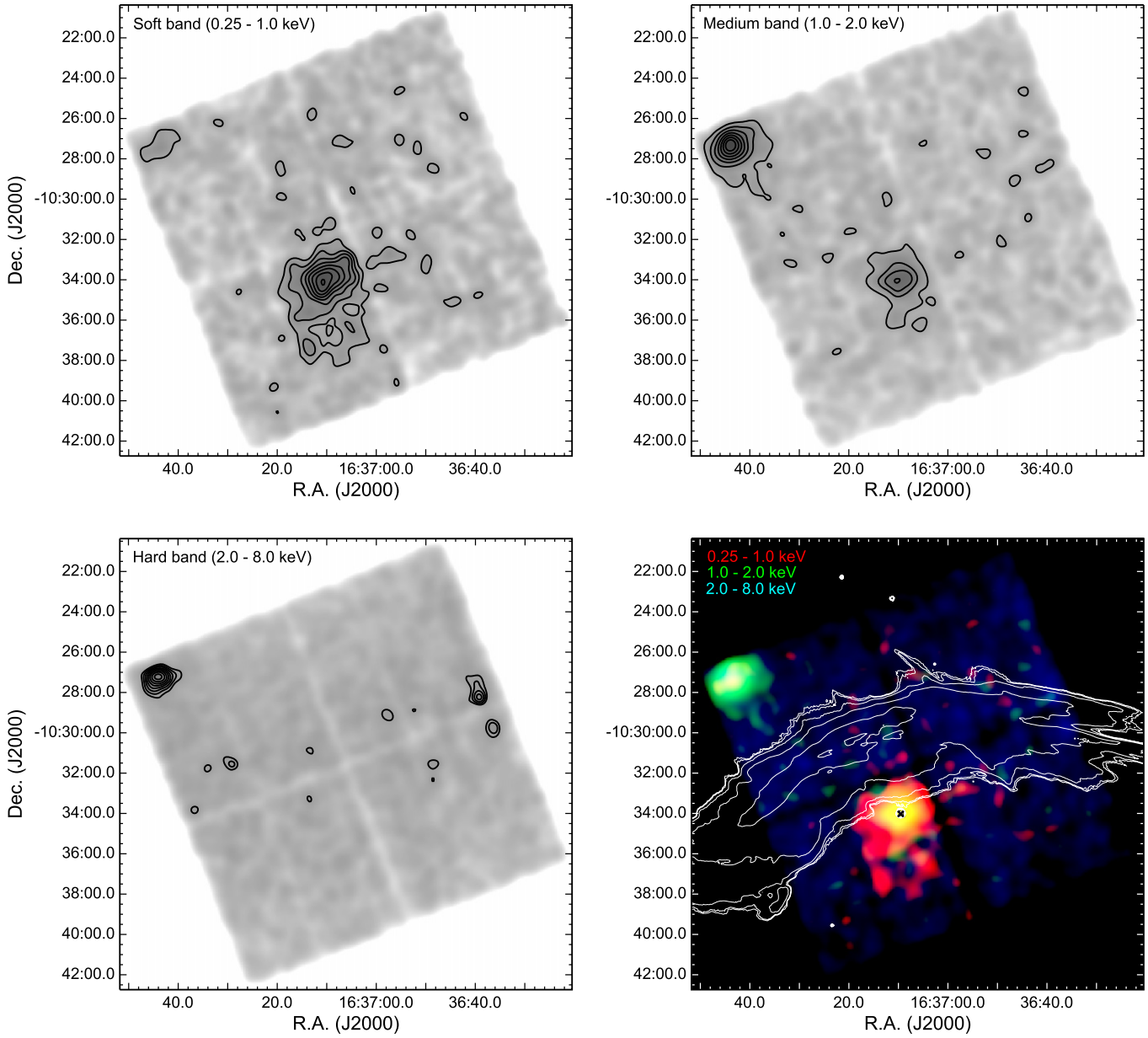

Figure 3. *Chandra* ACIS-I exposure-corrected, background-subtracted images of the X-ray emission around ζ Oph. The energy bands are labeled on each panel. The bottom right panel shows a composite color image of the three other panels, while contours show the *Spitzer* MIPS 24 μm emission from the bow shock. Point sources have been excised from these images, including the central star.

diffuse X-ray emission. The spectra of ζ Oph and its diffuse X-ray emission are presented in the top panels of Figure 5.

During the analysis of the *Chandra* data, we realized that the spectrum from ζ Oph suffered from the effect of pile-up. Because of this, we decided to analyze the archived *Suzaku* data of this source. We have extracted the XIS 0, XIS 1, and XIS 3 spectra from a circular apertures with radii of $4\farcm3$ centered at the position of ζ Oph, and the background region has been extracted from an annular region (see Appendix for details). The *Suzaku* XIS0, XIS1, and XIS3 spectra are shown in the bottom left panel of Figure 5.

As expected, the *Chandra* and *Suzaku* spectra of ζ Oph (Figure 5, left panels) present very similar features: a broad main feature centered at 0.9 keV with two secondary peaks around $\lesssim$1.4 and 1.8 keV and a rapid decay at energies greater than 3.0 keV. The spectrum of the apparently extended X-ray emission in vicinity of ζ Oph was extracted from the polygonal regions defined in the left panel of Figure 2, excising point-like sources present in these regions. The spectrum of extended emission is very similar to the spectrum of the central star (Figure 5, top right panel) with maximum of spectral energy distribution at about 0.9 keV and no significant count rate below 0.4 keV.

To study the physical properties of X-rays from ζ Oph and the associated extended X-ray emission, we have performed spectral analysis using XSPEC (v.12.8.2 Arnaud 1996). The fits were performed taking into account a Tuebingen-Boulder ISM absorption model as incorporated in XSPEC (Wilms et al. 2000). The abundances for the star and that of the diffuse emission were assumed to be the same. We assumed the C, N, and O abundances as those reported by Villamariz & Herrero (2005). The interstellar column density was fixed according to the known reddening of ζ Oph at $N_{\rm H} = 6 \times 10^{20}$ cm^{-2} (e.g., Liszt et al. 2009).

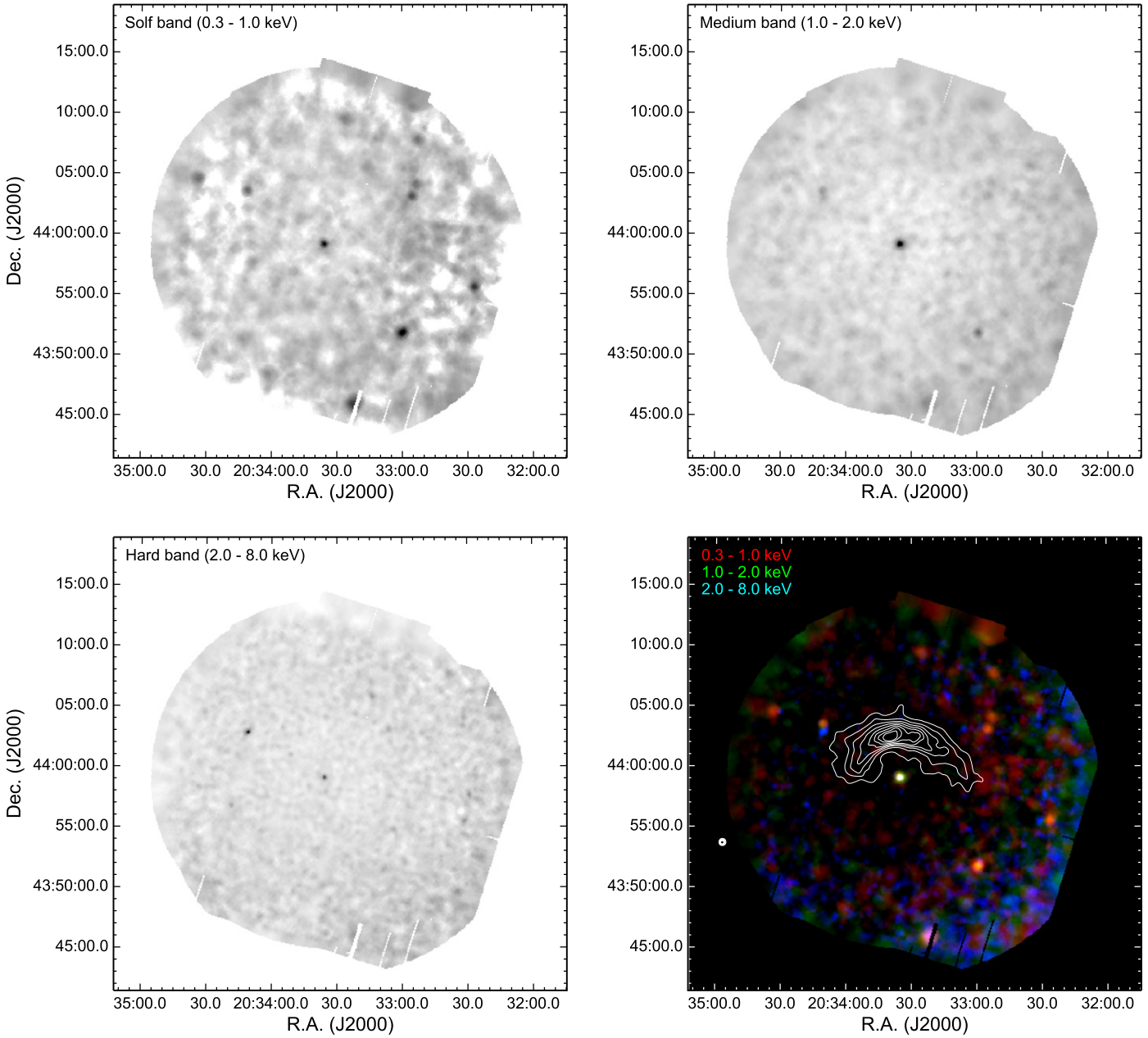

Figure 4. *XMM-Newton* EPIC (MOS+pn) exposure-corrected, background-subtracted images of the X-ray emission around BD+43°3654. The energy bands are labeled on each panel. The bottom right panel shows a composite color image of the three other panels, while contours show the *WISE* 22 μm emission from the bow shock. The star is centered on each panel. Unlike Figure 3, no point sources have been excised from these images.

We started our modeling of ζ Oph using a simple model and then increased its complexity. We have fit a (i) single *apec* plasma temperature, (ii) a two-temperature *apec* plasma model, (iii) a power-law model, (iv) a one-temperature *apec* plasma model plus a power-law component, and (iv) a two-power-law model. None of these combinations could fit the observed spectrum and they resulted in fits with reduced χ^2 greater than five, unless we include the effects of pile-up. Apparently the broad prominent spectral feature seen at around 1.8 keV is just a pile-up effect leading to the doubling of energies of photons at the maximum of spectral energy distribution around 0.9 keV. This is likely the reason that the 1.8 keV feature in the *Suzaku* spectra seems narrower, i.e., not affected by pile-up.

The best-fit model, taking into account the pile-up, resulted in a $\chi^2/\mathrm{dof} = 1.98$ and accounts for the contribution of a thermal component (an *apec* plasma model) and a power-law model (see Table 1). The plasma temperature is $kT = 0.80^{+0.02}_{-0.02}$ keV and the power-law index of $\Gamma = 3.05^{+0.10}_{-0.11}$. Surprisingly, models including one-plasma temperature (*apec*) or two-plasma temperature components (*apec* + *apec*) did not resulted in a good fit ($\chi^2 > 5$); thus, we do not list it in Table 1.

The absorbed and unabsorbed fluxes in the 0.4–4.0 keV energy range are $f = 2.10 \times 10^{-12}$ erg cm^{-2} s^{-1} and $F = 2.50 \times 10^{-12}$ erg cm^{-2} s^{-1}, respectively. The total X-ray luminosity at a distance of 222 pc (see Megier et al. 2009) is $L_{\mathrm{X}} = 1.5 \times 10^{31}$ erg s^{-1}.

Assuming that the extended X-ray emission is a combination of the spillover created by the pile-up and the diffuse X-ray emission we have used the best-fit model parameters of ζ Oph as components plus another component. We note that we used the same ratio of the normalization parameters from the central star ($A_1/A_2 = 0.93$). We found that the best-fit model was achieved

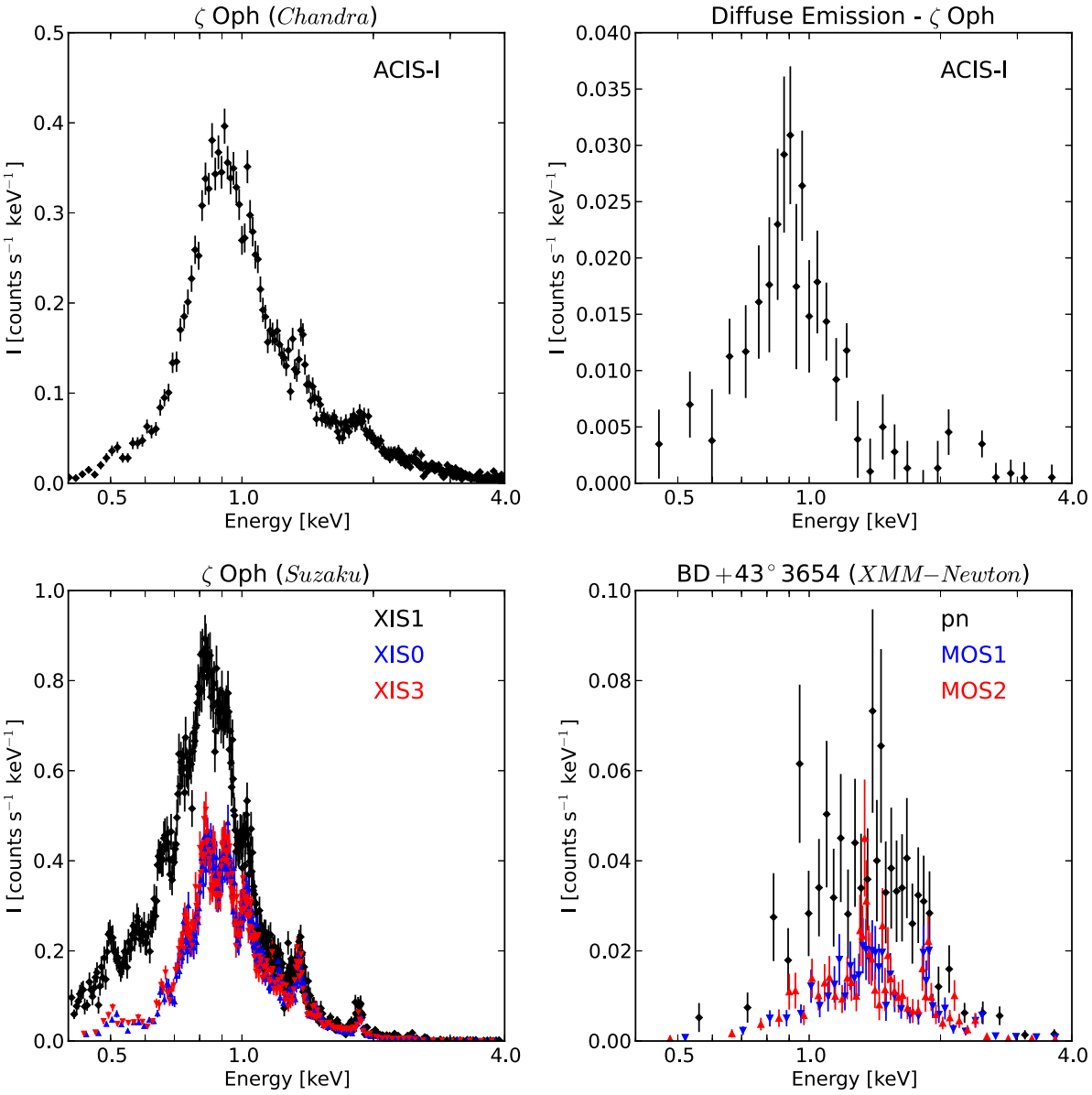

Figure 5. Background-subtracted spectra from different observations used in the present paper. *Chandra* ACIS-I spectra of ζ Oph (upper left panel) and its corresponding extended emission (upper right panel). The bottom left panel shows the spectra of ζ Oph obtained by the *Suzaku* cameras. The bottom right panel shows the spectra of BD+43°3654 obtained by the *XMM-Newton* EPIC cameras.

accounting for a two-temperature component ($apec_1 + apec_2$) and a fixed power law as obtained from ζ Oph model ($\Gamma = 3.05$; see Table 1). The plasma temperature of the diffuse X-ray emission was found to be $kT = 0.20^{+0.09}_{-0.07}$ keV ($T_X = 2.3 \times 10^6$ K). The absorbed and unabsorbed fluxes of this component resulted to be $f_{DIFF} = 8.4 \times 10^{-14}$ erg cm^{-2} s^{-1} and $F_{DIFF} = 1.30 \times 10^{-13}$ erg cm^{-2} s^{-1}. Its corresponding luminosity at a distance of 222 pc is $L_{DIFF} = 7.60 \times 10^{29}$ erg s^{-1}.

Finally, to assess the validity of the *Chandra* ACIS-I spectral fits, we also modeled the X-ray emission as detected by *Suzaku* (Figure 5, bottom left panel). These observations do not have the resolution to spatially separate the X-ray emission from ζ Oph and that of the extended emission. Thus, the *Suzaku* XIS0, XIS1, and XIS3 spectra include both the contribution of the central star and the putative diffuse emission.

First, we modeled the X-ray emission as detected by the back-illuminated CCD XIS 1. The best-fit model resulted in two *apec* components of $kT_1 = 0.21^{+0.01}_{-0.01}$ keV ($T = 2.4 \times 10^6$ K) and $kT_2 = 0.75^{+0.01}_{-0.01}$ keV (see Table 1). We then performed a joint fit to the three XIS cameras (XIS 0+XIS 1+XIS 3) and the best-fit model resulted in similar parameters (see Table 1). Thus, the *Suzaku* observations also point out at the existence of thermal plasma at $\sim 2 \times 10^6$ K gas while the second component, with a plasma temperature of $kT \approx 0.80$ keV, corresponds to ζ Oph.

3.2. X-rays from BD+43°3654

We do not detect any hint of diffuse X-ray emission associated to BD+43°3654 (see Figures 2 and 4) at the position of the bow shock as in the case of the non-thermal radio emission (e.g., Benaglia et al. 2010), nor at the position of the wake as in the case of ζ Oph.

In a similar way as in the previous section, we extracted pn, MOS1, and MOS2 spectra from a circular region with a radius of 20″ for the case of BD+43°3654. The background was extracted from a region with no contribution of point sources

Table 1
Best-fit Models for Spectra Obtained from *Chandra* and *Suzaku* Observations

						χ^2/dof
ζ Oph[a]						
	apec$_1$ $kT = 0.80^{+0.02}_{-0.02}$ keV $A_1 = 5.2 \times 10^{-4}$ cm^{-5}	+	Power law $\Gamma = 3.05^{+0.10}_{-0.11}$ $A_2 = 5.6 \times 10^{-4}$ cm^{-5}			1.98 = 236.23/119
Diffuse emission around ζ Oph						
	apec$_1$ $kT_1 = 0.75^{+0.10}_{-0.11}$ keV $A_1 = 3.4 \times 10^{-5}$ cm^{-5}	+	Power law $\Gamma = 3.05$ (fixed) $A_2 = 1.9 \times 10^{-5}$ cm^{-5}			1.24 = 38.52/31
	apec$_1$ $kT_1 = 0.85^{+0.20}_{-0.19}$ keV $A_1 = 2.0 \times 10^{-5}$ cm^{-5}	+	Power law $\Gamma = 3.05$ (fixed) $A_2 = 1.1 \times 10^{-5}$ cm^{-5}	+	*apec*$_2$ $kT_2 = 0.20^{+0.09}_{-0.07}$ keV $A_3 = 1.2 \times 10^{-4}$ cm^{-5}	1.05 = 30.58/29
ζ Oph+ Diffuse emission XIS1						
	apec$_1$ $kT_1 = 0.65^{+0.01}_{-0.01}$ keV $A_1 = 9.5 \times 10^{-4}$ cm^{-5}	+	Power law $\Gamma = 3.8^{+0.5}_{-0.5}$ $A_2 = 4.5 \times 10^{-4}$ cm^{-5}			1.91 = 2975/1556
XIS1						
	apec$_1$ $kT_1 = 0.75^{+0.01}_{-0.01}$ keV $A_1 = 9.3 \times 10^{-4}$ cm^{-5}			+	*apec*$_2$ $kT_2 = 0.21^{+0.01}_{-0.01}$ keV $A_3 = 2.1 \times 10^{-3}$ cm^{-5}	1.52 = 2371.61/1556
XIS0+XIS1+XIS3						
	apec$_1$ $kT_1 = 0.74^{+0.01}_{-0.01}$ keV $A_1 = 9.4 \times 10^{-4}$ cm^{-5}			+	*apec*$_2$ $kT_2 = 0.20^{+0.01}_{-0.01}$ keV $A_3 = 2.1 \times 10^{-3}$ cm^{-5}	1.50 = 5658.75/3769
XIS0+XIS1+XIS3						
	apec$_1$ $kT_1 = 0.77^{+0.01}_{-0.01}$ keV $A_1 = 7.2 \times 10^{-4}$ cm^{-5}	+	Power law $\Gamma = 3.43^{+0.10}_{-0.10}$ $A_2 = 3.1 \times 10^{-4}$ cm^{-5}	+	*apec*$_2$ $kT_2 = 0.24^{+0.01}_{-0.01}$ keV $A_3 = 1.4 \times 10^{-3}$ cm^{-5}	1.89 = 741.5/394

Note.
[a] Model performed accounting for the pile-up effect.

toward the south. The resultant background-subtracted EPIC (pn, MOS1, and MOS2) spectra are shown in the bottom right panel of Figure 5. The EPIC-pn spectrum exhibits a broad feature around 1.0–2.0 keV, but the MOS spectra present clearer emission features at 1.4 and 1.8 keV. No significant emission is detected below 0.4 keV or above 4.0 keV.

To produce the best-fit model of the X-ray emission from BD +43°3654, we have fitted the three EPIC spectra (pn, MOS1, and MOS2) simultaneously. We have used a one-temperature *apec* optically thin plasma model with solar abundances. We let the column density ($N_{\rm H}$) to be a free parameter in the fit as it unknown. The best-fit model resulted in an absorbing column density and plasma temperature of $N_{\rm H} = (1.54^{+0.08}_{-0.07}) \times 10^{22}$ cm^{-2} and $kT = 0.6^{+0.5}_{-0.4}$ keV with a χ^2/dof = 0.948. Note that Terada et al. (2012) found very similar values from their analysis of *Suzaku* observations. More sophisticated models, e.g., a two-temperature plasma emission model or a power-law contribution, did not improve the spectral fits; on the contrary, they resulted in models with χ^2/dof < 0.8.

The absorbed flux in the 0.4–4.0 keV energy range is $f = 1.20 \times 10^{-13}$ erg cm^{-2} s^{-1} that corresponds to an intrinsic flux of $F = 3.15 \times 10^{-12}$ erg cm^{-2} s^{-1}. The X-ray luminosity at a distance of 1.4 kpc (see Comerón & Pasquali 2007, and references therein) is $L_{\rm X} = 7.4 \times 10^{32}$ erg s^{-1}.

4. DISCUSSION

So far, high-energy, non-thermal emission is eluding detection in bow shocks around massive runaway O-type stars (e.g., Terada et al. 2012; Schulz et al. 2014; and this work). We would have expected that if present, non-thermal X-ray emission should be spatially coincident with the bow shock detected in mid-IR wavelengths, but this is not the case for the two objects studied in the present paper. In particular, the lack of non-thermal diffuse X-ray emission from BD+43°3654 is puzzling, as VLA observations assured the nature and presence of non-thermal particles. Although one might argue that the current *XMM-Newton* observations are not sensitive enough, Terada et al. (2012) did not find any signature of extended emission with their *Suzaku* observations as mentioned previously.

To set an upper limit to the non-thermal X-ray emission, we extracted the background-subtracted spectra of the two observations from regions spatially coincident of that of the bow shock, where the non-thermal emission is expected. The corresponding background count rate in the 0.4–4.0 keV energy range for ζ Oph and BD+43°3654 are 1.1×10^{-3} ACIS-I counts s^{-1} and 3.7×10^{-3} EPIC-pn counts s^{-1}, respectively. Using the *Chandra* PIMMS tool[7] we can estimate upper limits to the fluxes and

[7] http://cxc.harvard.edu/toolkit/pimms.jsp

luminosities. If we assume that the background emission can be modeled by a power-law spectrum with $\Gamma = 1.5$, the estimated upper limits to the absorbed (unabsorbed) fluxes for ζ Oph and BD+43°3654 are $9.5(10.6) \times 10^{-15}$ erg cm^{-2} s^{-1} and $1.5\ (3.6) \times 10^{-14}$ erg cm^{-2} s^{-1}, while their corresponding normalization parameters are 2.4×10^{-6} cm^{-5} and 8.2×10^{-6} cm^{-5}, respectively. The estimated upper limit to the X-ray luminosity in the 0.4–4.0 keV energy range is 6.2×10^{28} erg s^{-1} and 8.4×10^{30} erg s^{-1} for ζ Oph and BD+43°3654, respectively. Note that Terada et al. (2012) estimated an upper X-ray luminosity of 1.1×10^{32} erg s^{-1} for the 0.5–10 keV energy range for their *Suzaku* observations of BD+43°3654 for a photon index $\Gamma = 1.1$. If non-thermal X-ray emission is produced as suggested by analytical predictions (e.g., del Valle & Romero 2012), its intensity should be below the background detection levels of the current X-ray satellites.

Extreme care should be taken when considering the *Chandra* observations of ζ Oph, as they have been affected by pile-up. It must be noted that due to this effect, the final best-fit model of ζ Oph (*apec*+power law) is not to be taken as a definite physical parameter of the star (specifically the power-law component). This model should only be taken as the statistically best-fit model within the instrumental limitations. In any case, it helped us restrict the physical origin of the extended emission, a thermal nature, in addition with the analysis of the *Suzaku* data.

The soft plasma temperature of this extended X-ray emission ($T_X \approx 2 \times 10^6$ K) implies the existence of a mixing region between the adiabatically shocked wind region ($T = 10^7$–10^8 K) and the ionized outer material ($T \approx 10^4$ K), similar to that found in classic wind-blown bubbles (e.g., H II regions, planetary nebulae, Wolf–Rayet nebulae, and superbubbles; Chu et al. 2001; Güdel et al. 2008; Jaskot et al. 2011; Toalá et al. 2015). Simulations presented by Mackey et al. (2015) suggest that in the case of runaway stars, the most important mixing region is placed at the wake of the bow shock, which would produce a cometary-like distribution of X-ray-emitting gas. If this is the case for ζ Oph, it will be the first wind-blown bubble around a single O-type star with diffuse X-ray emission.

We have also examined the archived *Chandra* HETG observations of ζ Oph (Obs. ID:3857 and 2571) and found no evidence of this extended X-ray emission in the zero-order images.

Finally, it is interesting to discuss the absence of thermal X-ray emission at the wake of BD+43°3654. Even though this star has a greater mechanical wind luminosity than ζ Oph and can easily carve an adiabatically shocked hot bubble due to its high stellar wind velocity ($v_\infty \approx 2250$ km s^{-1}; see Section 1), it does not exhibit diffuse X-ray emission. This might be due to the fact that the wake region in BD+43°3654 seems to be more contaminated by ISM material in the line of sight than ζ Oph, as illustrated in Figure 1. Moreover, this region is detected at the edge of the EPIC cameras which have a reduce sensitivity as compared to the central regions.

5. CONCLUSIONS

We have presented *Chandra*, *Suzaku*, and *XMM-Newton* observations of the runaway O-type stars ζ Oph and BD+43° 3654 to investigate the presence of diffuse non-thermal X-ray emission associated to their bow shocks. We found no evidence of such X-ray emission associated to the bow shocks. Nevertheless, we have estimated upper limits for the non-thermal X-ray luminosity in the 0.4–4.0 keV energy range of 6.2×10^{28} erg s^{-1} and 8.4×10^{30} erg s^{-1} for ζ Oph and BD +43°3654, respectively.

Although our *Chandra* observations of ζ Oph suffered from pile-up, we are able to detect diffuse thermal emission with plasma temperature of $T_X \approx 2 \times 10^6$ K. The distribution and location of this diffuse X-ray emission in the wake of the bow shock provides observational support to the predictions of radiation-hydrodynamic results by Mackey et al. (2015). This makes ζ Oph the first wind-blown bubble around a single O-type star that exhibits diffuse X-ray emission.

Future deep *XMM-Newton* observations of the present sources could help improve our findings and put new observational constrains to the current growing body of theoretical models.

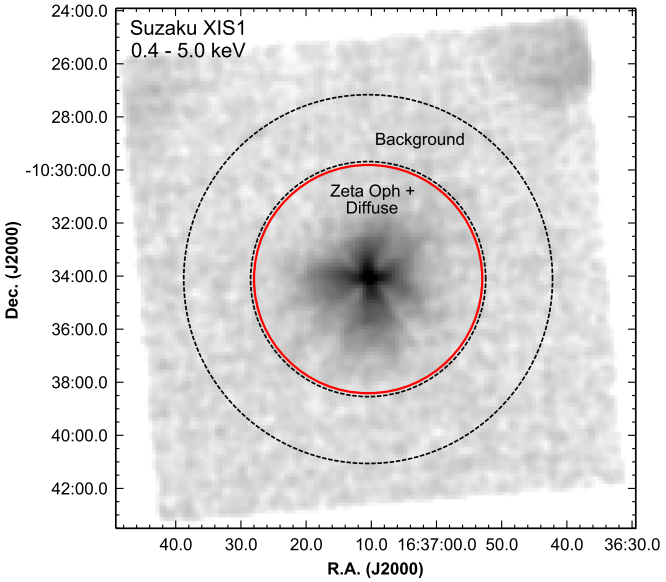

Figure 6. *Suzaku* XIS1 smoothed image of ζ Oph in the 0.4–5.0 keV energy range. The red solid line circle has a radius of 4.′3 and encloses the spectrum extraction region. The dashed-line annulus corresponds to the background region.

We thank the anonymous referee for helpful comments that helped improve our paper. J.A.T. and M.A.G. are supported by the Spanish MICINN (Ministerio de Ciencia e Innnovación) grant AYA 2014-57280-P. J.A.T. and L.M.O. acknowledge support from the ISM-SPP DFG Priority Program 1573. R.I. expresses appreciation for the support provided by the National Aeronautics and Space Administration through *Chandra* Award number G03-14008X, issued by the *Chandra X-ray Observatory* Center, which is operated by the Smithsonian Astrophysical Observatory for and on behalf of the National Aeronautics Space Administration under contract NAS8-03060.

APPENDIX
SUZAKU OBSERVATIONS

Figure 6 presents an image of the *Suzaku* XIS1 event file. The extraction region corresponds to a circular aperture of 4.′3 in radius centered at the position of ζ Oph. The background was extracted from an annular region with inner and outer radii of 4.′43 and 7′, respectively.

REFERENCES

Arnaud, K. A. 1996, in ASP Conf. Ser. 101, Astronomical Data Analysis, Software and Systems V, ed. G. H. Jacoby, & J. Barnes (San Francisco, CA: ASP), 17
Arthur, S. J., & Hoare, M. G. 2006, ApJS, 165, 283
Benaglia, P., Romero, G. E., Martí, J., Peri, C. S., & Araudo, A. T. 2010, A&A, 517, LL10
Blaauw, A. 1961, BAN, 15, 265
Brighenti, F., & D'Ercole, A. 1995a, MNRAS, 273, 443
Brighenti, F., & D'Ercole, A. 1995b, MNRAS, 277, 53
Chu, Y.-H., Guerrero, M. A., Gruendl, R. A., Williams, R. M., & Kaler, J. B. 2001, ApJL, 553, L69
Comeron, F., & Kaper, L. 1998, A&A, 338, 273
Comerón, F., & Pasquali, A. 2007, A&A, 467, L23
del Valle, M. V., & Romero, G. E. 2012, A&A, 543, AA56
del Valle, M. V., & Romero, G. E. 2014, A&A, 563, AA96
del Valle, M. V., Romero, G. E., & Santos-Lima, R. 2015, MNRAS, 448, 207
Fruscione, A., McDowell, J. C., Allen, G. E., et al. 2006, Proc. SPIE, 6270, 62701V
Fujii, M. S., & Portegies Zwart, S. 2011, Sci, 334, 1380
Gies, D. R., & Bolton, C. T. 1986, ApJS, 61, 419
Güdel, M., Briggs, K. R., Montmerle, T., et al. 2008, Sci, 319, 309
Gvaramadze, V. V., Langer, N., & Mackey, J. 2012, MNRAS, 427, L50
Hoogerwerf, R., de Bruijne, J. H. J., & de Zeeuw, P. T. 2000, ApJL, 544, L133
Huenemoerder, D. P., Oskinova, L. M., Ignace, R., et al. 2012, ApJL, 756, L34
Huthoff, F., & Kaper, L. 2002, A&A, 383, 999
Jaskot, A. E., Strickland, D. K., Oey, M. S., Chu, Y.-H., & García-Segura, G. 2011, ApJ, 729, 28
Kaper, L., van Loon, J. T., Augusteijn, T., et al. 1997, ApJL, 475, L37
Kobulnicky, H. A., Gilbert, I. J., & Kiminki, D. C. 2010, ApJ, 710, 549
Liszt, H. S., Pety, J., & Tachihara, K. 2009, A&A, 499, 503
López-Santiago, J., Miceli, M., del Valle, M. V., et al. 2012, ApJL, 757, L6
Mackey, J., Gvaramadze, V. V., Mohamed, S., & Langer, N. 2015, A&A, 573, A10
Marcolino, W. L. F., Bouret, J.-C., Martins, F., et al. 2009, A&A, 498, 837
Megier, A., Strobel, A., Galazutdinov, G. A., & Krełowski, J. 2009, A&A, 507, 833
Meyer, D. M.-A., Langer, N., Mackey, J., Velázquez, P. F., & Gusdorf, A. 2015, MNRAS, 450, 3080
Noriega-Crespo, A., van Buren, D., & Dgani, R. 1997, AJ, 113, 780
Oskinova, L. M., Hamann, W.-R., & Feldmeier, A. 2007, A&A, 476, 1331
Peri, C. S., Benaglia, P., Brookes, D. P., Stevens, I. R., & Isequilla, N. L. 2012, A&A, 538, AA108
Schulz, A., Ackermann, M., Buehler, R., Mayer, M., & Klepser, S. 2014, A&A, 565, A95
Šurlan, B., Hamann, W.-R., Aret, A., et al. 2013, A&A, 559, A130
Terada, Y., Tashiro, M. S., Bamba, A., et al. 2012, PASJ, 64, 138
Tetzlaff, N., Neuhäuser, R., & Hohle, M. M. 2011, MNRAS, 410, 190
Toalá, J. A., Guerrero, M. A., Chu, Y.-H., & Gruendl, R. A. 2015, MNRAS, 446, 1083
Ueda, Y., Ishisaki, Y., Takahashi, T., Makishima, K., & Ohashi, T. 2001, ApJS, 133, 1
van Buren, D., & McCray, R. 1988, ApJL, 329, L93
van Buren, D., Noriega-Crespo, A., & Dgani, R. 1995, AJ, 110, 2914
Villamariz, M. R., & Herrero, A. 2005, A&A, 442, 263
Wilms, J., Allen, A., & McCray, R. 2000, ApJ, 542, 914